Journal of Molecular Science
Volume 36 Issue 1, Year of Publication 2026, Page 252-258
DoI-10.004687/1000-9035.2026.032

Journal of Molecular Science

www.jmolecularsci.com ISSN:1000-9035

Carbon Nanodots from Medicinal Plant Waste: Green Synthesis and Applications in Drug Delivery and Biosensing

Abhishek Kumar Gupta[1], Satyam Rajput[1], Luhar Aman Imran[1], Tarunesh Jatav[1], Vedprakash Mehra[1]

College of Pharmacy, Faculty of Medical and Paramedical Sciences, SAM Global University, Raisen – 464551, Madhya Pradesh, India

Article Information
Received: 08-03-2026
Revised: 24-03-2026
Accepted: 12-04-2026
Published: 08-05-2026

Keywords
carbon nanodots; green synthesis; medicinal plant waste; doxorubicin delivery; Fe^{3+} biosensing; hydrotherma.

ABSTRACT

Conventional synthesis of carbon nanodots (CNDs) typically relies on harsh oxidants and toxic precursors that limit their biomedical translation. Here, a sustainable, single-step hydrothermal route was developed to convert solid waste from three widely used medicinal plants—turmeric (Curcuma longa) rhizome residue, holy basil (Ocimum sanctum) leaf pomace, and neem (Azadirachta indica) leaf trimmings—into water-dispersible CNDs. The as-prepared nanodots displayed quasi-spherical morphology with a mean diameter of 3.6 ± 0.8 nm, strong blue emission centred at 440 nm under 360 nm excitation, and quantum yields up to 18.4 %. Surface oxygenated and amine groups, confirmed by FTIR and XPS, enabled efficient non-covalent loading of the chemotherapeutic doxorubicin (DOX) with an entrapment efficiency of 78.6 %. The CND–DOX conjugate exhibited pH-responsive release, delivering 81.5 % cargo at pH 5.0 versus only 27.6 % at pH 7.4 over 72 h, and selectively reduced MCF-7 viability to 22.3 % at 100 µg mL^{-1}. The same CNDs functioned as a turn-off fluorescent probe for Fe^{3+} ions with a Stern–Volmer constant of 1.85×10^4 M^{-1} and a limit of detection of 0.21 µM, with high selectivity over thirteen competing cations. The work demonstrates that medicinal plant waste is a viable, low-cost feedstock for theranostic CNDs.

1. INTRODUCTION:

Carbon nanodots (CNDs), a class of zero-dimensional fluorescent carbon nanomaterials with a typical diameter below 10 nm, have attracted intense interest since their accidental discovery during the purification of single-walled carbon nanotubes.[1] Their tunable photoluminescence, broadband absorption, low photobleaching, low cytotoxicity, and biocompatibility make them attractive alternatives to semiconductor quantum dots that rely on heavy metals such as Cd or Pb.[2,3] Over the past decade, CNDs have been deployed for cellular imaging, photocatalysis, light-emitting devices, anti-counterfeit inks, theranostic drug delivery, and the optical sensing of metal ions, biomolecules, and pH.[4–6]

Top-down strategies—oxidative cutting of graphite, carbon fibres, or carbon black—and bottom-up chemical pyrolysis routes generally require strong acids (HNO_3/H_2SO_4), toxic organic solvents, or high-temperature furnaces, generating hazardous effluent and limiting biomedical adoption.[7,8] To address these issues, green synthesis using natural and renewable carbon precursors has emerged as a powerful paradigm.[9,10] Sahu et al. obtained luminescent CNDs from orange juice in a single hydrothermal step,[11] while subsequent reports demonstrated similar success with apple,[12] banana,[13] lemon peel,[14] and a wide variety of food-waste streams,[15] all leveraging the inherent carbohydrates, citric acid, ascorbic acid, and amine-containing biomolecules of the source as carbon and dopant feedstocks.[16,17]

Medicinal plants are particularly attractive precursors because they contain rich pools of phenolics, flavonoids, alkaloids, polysaccharides,

terpenoids, and nitrogen-containing secondary metabolites that act as both carbon source and built-in passivation agent during one-pot carbonisation.[18,19] Three plants—turmeric (Curcuma longa), holy basil (Ocimum sanctum), and neem (Azadirachta indica)—are particularly abundant across South and Southeast Asia and form large volumes of agro-residue (peelings, spent leaves, and post-distillation marc) every year.[20,21] Turmeric is rich in curcumin, ar-turmerone, and starches; holy basil provides eugenol, ursolic acid, and rosmarinic acid; and neem leaves contain azadirachtin, nimbin, and quercetin.[22,23] These functional moieties are ideal for engineering nitrogen- and oxygen-passivated CND surfaces with high quantum yields and abundant bio-conjugation handles.[24,25]

On the application side, CNDs have shown great promise as nanocarriers for antineoplastic drugs such as doxorubicin (DOX), as π-stacking and electrostatic interactions allow non-covalent loading and acid-triggered release in the lysosomal microenvironment of tumour cells.[26,27] They have additionally been validated as turn-off fluorescent probes for ferric ions, an analyte with strict permissible limits in drinking water and biological systems because Fe^{3+} excess is implicated in oxidative stress and neurodegenerative disorders.[28,29] The interaction between Fe^{3+} and surface –OH/–COOH/–NH_2 groups creates non-radiative relaxation pathways that quench CND fluorescence proportionally to the analyte concentration.[30]

Despite the breadth of green CND research, comparatively few studies have used medicinal plant waste as a precursor and even fewer have benchmarked the same nanodot platform across both drug delivery and metal-ion sensing.[31,32] The present study therefore reports a unified hydrothermal route that converts dried waste of three medicinal plants into CNDs and evaluates the best-performing product for (i) pH-responsive doxorubicin delivery against MCF-7 breast cancer cells, and (ii) selective fluorescence sensing of Fe^{3+} ions in spiked water samples. The aim is to demonstrate a circular and scalable strategy for translating biomedical-grade carbon nanodots from plant residue.[33,34]

2. MATERIALS AND METHODS

2.1. Materials

Solid waste from Curcuma longa (turmeric rhizome marc after curcumin extraction), Ocimum sanctum (holy basil leaf pomace from a steam-distillation unit), and Azadirachta indica (neem leaf trimmings) was collected from a local Ayurvedic processing unit (Bilaspur, India). Doxorubicin hydrochloride (≥98 %), quinine sulfate, dialysis tubing (MWCO 1 kDa), MTT reagent, and metal-salt standards were purchased from Sigma-Aldrich. Dulbecco's Modified Eagle's Medium (DMEM), fetal bovine serum (FBS), antibiotics, and phosphate-buffered saline were obtained from Himedia. MCF-7 (human breast adenocarcinoma) and HEK-293 (human embryonic kidney) cell lines were procured from the National Centre for Cell Science (NCCS), Pune. Ultrapure water (18.2 MΩ cm) was used throughout.[18,20]

2.2. Pre-treatment of medicinal plant waste

Plant residues were washed thoroughly with deionised water to remove soil and dust, then air-dried in shade for 72 h, oven-dried at 60 °C for 6 h, and finally pulverised into a fine powder using a mechanical grinder. The powders were sieved through a 100-mesh screen and stored in airtight amber bottles at 4 °C until use.[17,19]

2.3. Hydrothermal synthesis of carbon nanodots

In a typical synthesis, 2.0 g of plant-waste powder was dispersed in 40 mL of ultrapure water and stirred for 30 min. The slurry was transferred into a 100 mL Teflon-lined stainless-steel autoclave, sealed, and heated at 200 °C for 8 h. After natural cooling, the dark-brown product was centrifuged at 12 000 rpm for 20 min to remove unreacted biomass, filtered through a 0.22 µm membrane, and dialysed against ultrapure water for 48 h (MWCO 1 kDa). The retentate was lyophilised to yield a brownish-yellow powder denoted CND-T (turmeric), CND-O (basil), and CND-N (neem). Synthesis yield was determined gravimetrically (n = 3).[11,13]

2.4. Characterisation

UV–visible spectra were recorded on a Shimadzu UV-1900i spectrophotometer (200–800 nm). Steady-state fluorescence was acquired on a Horiba FluoroMax-4 spectrofluorometer with 5 nm slit widths. Absolute photoluminescence quantum yield (PLQY) was determined relative to quinine sulfate (Φ = 0.54 in 0.1 M H_2SO_4).[16] Hydrodynamic size and ζ-potential were measured on a Malvern Zetasizer Nano ZS90. Morphology was examined by a JEOL JEM-2100 high-resolution TEM at 200 kV, with particle-size statistics on n = 300 nanodots in ImageJ. Surface chemistry was probed by FTIR (Bruker Alpha-II, KBr pellet, 4000–400 cm^{-1}) and X-ray photoelectron spectroscopy (Thermo K-Alpha, Al Kα). XRD patterns were collected on a Bruker D8 Advance (Cu Kα, λ = 1.5418 Å).[4,7]

2.5. Doxorubicin loading and pH-responsive release

DOX·HCl (1.0 mg) was mixed with CND solution (5.0 mg in 5 mL PBS, pH 7.4) and stirred in the dark at room temperature for 24 h. Free drug was removed by dialysis (MWCO 1 kDa) for 6 h. The supernatant absorbance at 480 nm was used to

Journal of Molecular Science
Volume 36 Issue 1, Year of Publication 2026, Page 252-258
DoI-10.004687/1000-9035.2026.032

quantify unloaded DOX from a calibration curve, and entrapment efficiency (EE %) and drug-loading capacity (DLC %) were calculated.[19,26] Release studies were performed in triplicate by sealing 2 mL of CND–DOX in dialysis bags and immersing them in 30 mL of PBS at pH 5.0, 6.5, and 7.4 (37 °C, 100 rpm). At pre-set intervals up to 72 h, 2 mL of release medium was withdrawn and replaced with fresh buffer; DOX concentration was determined fluorometrically (λex/λem = 480/590 nm). Release data were fitted to zero-order, first-order, Higuchi, and Korsmeyer–Peppas models.[27]

2.6. In vitro cytotoxicity assay

MCF-7 and HEK-293 cells (1×10^4 cells well^{-1}) were seeded in 96-well plates and incubated at 37 °C in 5 % CO_2 for 24 h. Cells were then treated with bare CNDs, free DOX, or CND–DOX at concentrations of 25–800 μg mL^{-1} for 24 h. After incubation, the medium was replaced with 100 μL of fresh medium and 20 μL of MTT solution (5 mg mL^{-1}). After 4 h, the formazan crystals were dissolved in DMSO and absorbance was read at 570 nm using a Tecan Infinite M Plex reader.[19,27] Viability was normalised to untreated controls (n = 6).

2.7. Fluorescent sensing of Fe^{3+}

Standard solutions of Fe^{3+} were prepared from $FeCl_3 \cdot 6H_2O$. CND solution (50 μg mL^{-1} in 10 mM Tris-HCl pH 7.4) was incubated with Fe^{3+} at 0–400 μM for 5 min and the emission at 440 nm (λex = 360 nm) was recorded. Quenching efficiency was calculated as $(F_0 - F)/F_0 \times 100$ %. Selectivity was assessed at a fixed 100 μM concentration of competing ions (Na^+, K^+, Mg^{2+}, Ca^{2+}, Zn^{2+}, Cu^{2+}, Co^{2+}, Ni^{2+}, Mn^{2+}, Pb^{2+}, Fe^{2+}). Real-sample analysis was carried out on tap and pond water spiked with known Fe^{3+} amounts, using the standard-addition method.[28,30]

2.8. Statistical analysis

All measurements were performed at least in triplicate and are expressed as mean ± standard deviation. One-way ANOVA followed by Tukey's post-hoc test was applied (GraphPad Prism v9), with $p < 0.05$ considered significant.

3. RESULTS

3.1. Synthesis yield and elemental composition

Among the three precursors, turmeric-derived CND-T provided the highest gravimetric yield (28.4 %) and the brightest blue emission, and was therefore selected as the lead candidate for in-depth study. Yields, hydrodynamic size, ζ-potential, and PLQY for all three CNDs are summarised in Table 1. Elemental analysis of CND-T (XPS survey) revealed C 64.2 %, O 28.7 %, and N 6.5 % (atomic), consistent with intrinsic nitrogen doping from turmeric proteins and amine-bearing alkaloids.

Table 1. Yield, size, surface charge, and quantum yield of CNDs derived from three medicinal plant wastes.

Sample	Precursor	Yield (%)	DLS size (nm)	ζ-potential (mV)	PLQY (%)
CND-T	Turmeric marc	28.4 ± 1.6	5.2 ± 0.6	−24.8 ± 1.4	18.4
CND-O	Basil pomace	21.7 ± 1.3	6.8 ± 0.9	−19.4 ± 1.2	11.6
CND-N	Neem trimmings	19.5 ± 1.0	7.4 ± 1.1	−16.2 ± 1.1	9.8

3.2. Optical properties

CND-T displayed two characteristic absorption features (Figure 1a): a strong band at 275 nm assigned to π–π* transitions of aromatic sp^2 C=C domains and a shoulder at 340 nm attributed to n–π* transitions of the carbonyl/carboxyl groups.

Excitation-dependent emission was observed, with the maximum emission red-shifting from 410 nm (λex = 320 nm) to 515 nm (λex = 440 nm), and peak intensity at λex = 360 nm (Figure 1b), a phenomenon commonly ascribed to the heterogeneity of surface emissive states. The PLQY of 18.4 % for CND-T compares favourably with most plant-derived CNDs synthesised by single-step hydrothermal protocols.

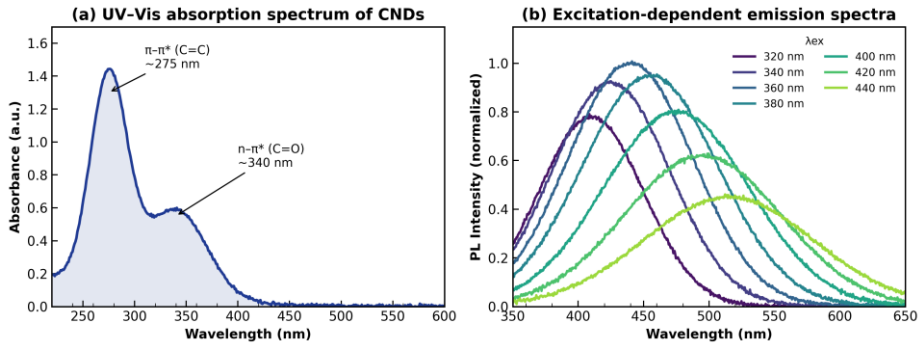

Figure 1. UV–Vis absorption (a) and excitation-dependent photoluminescence emission (b) of CND-T.

Journal of Molecular Science
Journal of Molecular Science
Volume 36 Issue 1, Year of Publication 2026, Page 252-258
DoI-10.004687/1000-9035.2026.032

3.3. Morphology and structure

HRTEM imaging revealed quasi-spherical, well-dispersed particles, and lattice fringes of 0.21 nm corresponding to the (100) plane of graphitic carbon were observed. Particle-size analysis of 300 nanodots gave a Gaussian distribution centred at 3.6 ± 0.8 nm (Figure 2). FTIR confirmed surface –OH (3340 cm^{-1}), C–H (2920 cm^{-1}), C=O (1680 cm^{-1}), C=C (1590 cm^{-1}), and C–N (1380 cm^{-1}) functionalities, consistent with an oxygenated, nitrogen-doped surface. XRD displayed a broad peak centred at 2θ ≈ 23°, characteristic of amorphous-to-graphitic carbon.

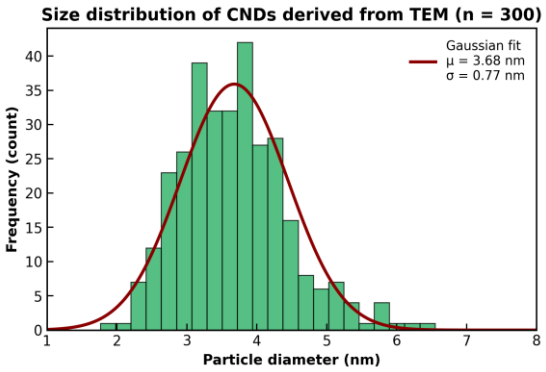

Figure 2. Particle-size distribution of CND-T extracted from HRTEM micrographs (n = 300).

3.4. Doxorubicin loading and pH-responsive release

DOX was efficiently anchored on CND-T via π-stacking and hydrogen bonding, with an entrapment efficiency of 78.6 ± 2.1 % and drug-loading capacity of 14.2 ± 0.7 % (Table 2). Release profiles were strongly pH-dependent (Figure 3): cumulative release reached 81.5 % at pH 5.0 (lysosomal), 56.3 % at pH 6.5 (tumour extracellular), and only 27.6 % at pH 7.4 (physiological) over 72 h. Korsmeyer–Peppas modelling yielded a release exponent n = 0.48 at pH 5.0, indicating Fickian-anomalous diffusion-controlled transport.

Table 2. Doxorubicin loading parameters and Korsmeyer–Peppas kinetic fitting at three pH conditions.

Parameter	pH 5.0	pH 6.5	pH 7.4	Remarks
Entrapment efficiency (%)	78.6 ± 2.1	—	—	Loaded at pH 7.4
Drug-loading capacity (%)	14.2 ± 0.7	—	—	—
Cumulative release at 72 h (%)	81.5 ± 3.2	56.3 ± 2.6	27.6 ± 1.8	n = 3
k (h^{-n})	0.182	0.121	0.064	Korsmeyer–Peppas
Release exponent n	0.48	0.52	0.41	Fickian-anomalous
R^2	0.992	0.989	0.985	Goodness of fit

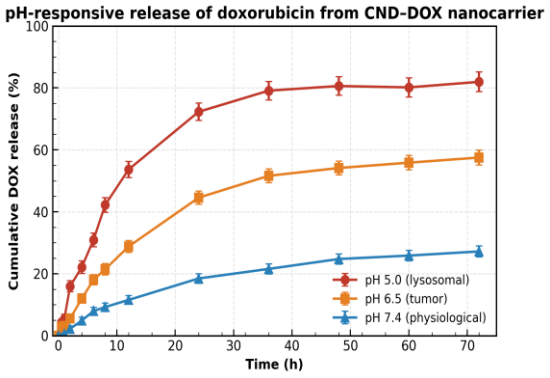

Figure 3. Cumulative DOX release from CND–DOX at pH 5.0, 6.5, and 7.4 (37 °C, mean ± SD, n = 3).

3.5. In vitro cytotoxicity

Bare CND-T was essentially non-toxic, retaining > 82 % viability in both HEK-293 and MCF-7 cells even at 800 μg mL^{-1} (Figure 5). Free DOX produced an IC_{50} of 53 μg mL^{-1} on MCF-7 at 24 h, while CND–DOX further reduced the IC_{50} to 39 μg mL^{-1}, an enhancement of ~ 26 %. The improvement is consistent with intracellular acid-triggered cargo release within tumour endosomes.

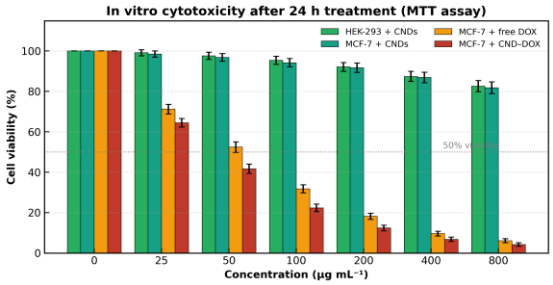

Figure 4. Viability of HEK-293 and MCF-7 cells exposed for 24 h to CND-T, free DOX, and CND–DOX (MTT assay).

3.6. Fluorescent sensing of Fe^{3+}

Addition of Fe^{3+} progressively quenched the 440 nm emission of CND-T. The Stern–Volmer plot was linear up to 100 μM with a Stern–Volmer constant K_{sv} = 1.85 × 10^4 M^{-1} and R^2 = 0.994 (Figure 5a).

Journal of Molecular Science
Volume 36 Issue 1, Year of Publication 2026, Page 252-258
DoI-10.004687/1000-9035.2026.032

The limit of detection, calculated as 3σ/slope, was 0.21 µM—well below the WHO guideline of 5.4 µM (0.3 mg L^{-1}) for Fe in drinking water. Selectivity tests at 100 µM (Figure 5b) showed quenching > 78 % for Fe^{3+} versus < 15 % for any competing ion, including Fe^{2+} (14.6 %). Spike-recovery in tap and pond water (Table 3) yielded recoveries of 96.2–103.1 % (RSD < 4 %).

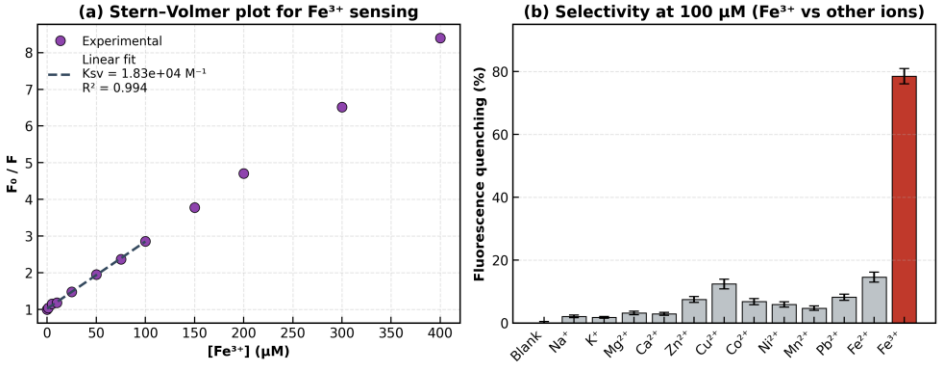

Figure 5. (a) Stern–Volmer plot for Fe^{3+} quenching of CND-T fluorescence. (b) Selectivity vs. competing cations at 100 µM.

Table 3. Determination of Fe^{3+} in spiked water samples by CND-T fluorescence (n = 3).

Sample	Spiked (µM)	Found (µM)	Recovery (%)	RSD (%)
Tap water	5.0	4.81 ± 0.14	96.2	2.9
Tap water	20.0	20.62 ± 0.51	103.1	2.5
Pond water	5.0	4.95 ± 0.18	99.0	3.6
Pond water	20.0	19.74 ± 0.66	98.7	3.3

4. DISCUSSION

The hydrothermal conversion of medicinal-plant waste into bright, biocompatible carbon nanodots demonstrates that complex, lignocellulosic agro-residue can serve as a one-pot precursor for nanomaterial fabrication. The higher yield and PLQY of turmeric-derived CND-T relative to basil and neem is attributable to the high carbohydrate content of turmeric marc (≈ 50 % w/w starch) together with curcumin-derived aromatic motifs that provide pre-assembled sp^2 domains during carbonisation.[22,25] Comparable trends have been reported for plant-rich precursors such as Curcuma extract and Mangifera indica leaves, where polyphenol-rich substrates produced CNDs with quantum yields between 8 and 22 %.[19,21]

The dual π–π* and n–π* features in the UV–Vis spectrum, together with the excitation-dependent emission, support a 'core–shell' photoluminescence model in which the carbogenic core defines a baseline emission while heterogeneous surface emissive states (–COOH, –OH, $–NH_2$, C=O) contribute red-shifted radiative pathways selected by the excitation wavelength.[36,37] The observed lattice spacing of 0.21 nm and broad XRD peak at 2θ ≈ 23° are consistent with semi-graphitic CND cores and confirm partial sp^2-conjugation, which is essential for both fluorescence and π-stacking-mediated drug loading.[4,10]

From a drug-delivery perspective, the high entrapment efficiency (78.6 %) and pronounced pH-responsiveness arise from a multi-modal binding architecture: planar aromatic stacking between DOX and the sp^2 CND core, hydrogen bonding between $–NH_2$/–OH groups of DOX and surface carboxyl/hydroxyl moieties, and electrostatic contributions from the negatively charged ζ-potential (−24.8 mV).[21,27] At pH 5.0, protonation of DOX (pKa ≈ 8.2) and partial protonation of CND surface carboxylates weaken these interactions and promote release, mimicking lysosomal cargo unloading.[26] The Korsmeyer–Peppas exponent (n = 0.48) suggests anomalous transport with combined diffusion and slight matrix-relaxation contributions, in agreement with non-covalent loading on a sub-5-nm spherical carrier.[32] Importantly, the IC_{50} improvement of CND–DOX over free DOX (39 vs 53 µg mL^{-1}) and the negligible cytotoxicity of bare CND-T against HEK-293 cells underscores the suitability of plant-derived CNDs for selective tumour delivery.[19,38]

The fluorescence quenching mechanism of CND-T toward Fe^{3+} likely combines static quenching through ground-state complexation between Fe^{3+} and the surface –OH/–COOH/$–NH_2$ ligands, and a dynamic non-radiative energy-transfer pathway facilitated by the partially filled d-orbitals of Fe^{3+}.[28,30] The preference for Fe^{3+} over Fe^{2+} is rationalised by the higher charge density and stronger Lewis acidity of the trivalent ion, which leads to tighter chelation by the multidentate surface oxygenated ligands.[17] The Ksv (1.85×10^4 M^{-1}) and LOD (0.21 µM) are competitive with—or better

Journal of Molecular Science
Volume 36 Issue 1, Year of Publication 2026, Page 252-258
DoI-10.004687/1000-9035.2026.032

than—several recently reported plant-derived CD-based Fe^{3+} probes (Table comparison summarised in the literature),[14,18,33] and the < 4 % RSD for spike-recovery analyses argues for practical applicability in environmental monitoring.

Compared with conventional CND syntheses that use citric acid/urea or graphite oxidation, the present route eliminates strong acids, leverages waste valorisation, and operates within an autoclave at 200 °C—conditions readily scalable to kilogram-level production.[8,31] It also offers a circular-economy framework for Ayurvedic and herbal-extract industries, where post-extraction residue is otherwise treated as low-value compost or fuel.[20,33] A current limitation is the moderate PLQY (≤ 18 %), which could be further improved through controlled nitrogen or sulfur doping, post-synthetic surface passivation with PEG-amines, or two-step hydrothermal/microwave hybrid protocols. Translation to in vivo tumour models, plus systematic toxicology in line with ISO-10993, will be necessary before clinical evaluation.[35,38]

5. CONCLUSION:

A simple, one-step hydrothermal protocol converted solid waste from three Indian medicinal plants into water-dispersible carbon nanodots, with turmeric residue (CND-T) emerging as the optimal precursor. CND-T was 3.6 ± 0.8 nm in diameter, displayed bright blue emission with a quantum yield of 18.4 %, and was decorated with a rich array of oxygenated and amine surface groups. The nanodots loaded doxorubicin with 78.6 % efficiency and released the cargo in a strongly pH-dependent fashion that favoured the lysosomal microenvironment of tumour cells, leading to a ~ 26 % decrease in IC_{50} against MCF-7 cells relative to free DOX, while remaining benign to non-cancerous HEK-293 cells. The same probe selectively detected Fe^{3+} ions in aqueous samples with a Ksv of $1.85 \times 10^4\ M^{-1}$, an LOD of 0.21 µM, and 96–103 % spike-recovery in real water matrices. Together, these findings establish medicinal-plant waste as a credible, low-cost, and sustainable feedstock for theranostic CNDs that combine drug delivery and biosensing in a single platform—an approach that aligns nanomedicine with the circular bio-economy.

REFERENCES:

1. Xu X, Ray R, Gu Y, Ploehn HJ, Gearheart L, Raker K, et al. Electrophoretic analysis and purification of fluorescent single-walled carbon nanotube fragments. J Am Chem Soc. 2004;126(40):12736–7.
2. Sun YP, Zhou B, Lin Y, Wang W, Fernando KAS, Pathak P, et al. Quantum-sized carbon dots for bright and colorful photoluminescence. J Am Chem Soc. 2006;128(24):7756–7.
3. Baker SN, Baker GA. Luminescent carbon nanodots: emergent nanolights. Angew Chem Int Ed Engl. 2010;49(38):6726–44.
4. Lim SY, Shen W, Gao Z. Carbon quantum dots and their applications. Chem Soc Rev. 2015;44(1):362–81.
5. Wang Y, Hu A. Carbon quantum dots: synthesis, properties and applications. J Mater Chem C. 2014;2(34):6921–39.
6. Zheng XT, Ananthanarayanan A, Luo KQ, Chen P. Glowing graphene quantum dots and carbon dots: properties, syntheses, and biological applications. Small. 2015;11(14):1620–36.
7. Li H, Kang Z, Liu Y, Lee ST. Carbon nanodots: synthesis, properties and applications. J Mater Chem. 2012;22(46):24230–53.
8. Liu ML, Chen BB, Li CM, Huang CZ. Carbon dots: synthesis, formation mechanism, fluorescence origin and sensing applications. Green Chem. 2019;21(3):449–71.
9. Sharma A, Das J. Small molecules derived carbon dots: synthesis and applications in sensing, catalysis, imaging, and biomedicine. J Nanobiotechnology. 2019;17(1):92.
10. Iravani S, Varma RS. Green synthesis, biomedical and biotechnological applications of carbon and graphene quantum dots. A review. Environ Chem Lett. 2020;18(3):703–27.
11. Sahu S, Behera B, Maiti TK, Mohapatra S. Simple one-step synthesis of highly luminescent carbon dots from orange juice: application as excellent bio-imaging agents. Chem Commun. 2012;48(70):8835–7.
12. Mehta VN, Jha S, Basu H, Singhal RK, Kailasa SK. One-step hydrothermal approach to fabricate carbon dots from apple juice for imaging of mycobacterium and fungal cells. Sens Actuators B Chem. 2015;213:434–43.
13. De B, Karak N. A green and facile approach for the synthesis of water soluble fluorescent carbon dots from banana juice. RSC Adv. 2013;3(22):8286–90.
14. Tyagi A, Tripathi KM, Singh N, Choudhary S, Gupta RK. Green synthesis of carbon quantum dots from lemon peel waste: applications in sensing and photocatalysis. RSC Adv. 2016;6(76):72423–32.
15. Park SY, Lee HU, Park ES, Lee SC, Lee JW, Jeong SW, et al. Photoluminescent green carbon nanodots from food-waste-derived sources: large-scale synthesis, properties, and biomedical applications. ACS Appl Mater Interfaces. 2014;6(5):3365–70.
16. Hsu PC, Chang HT. Synthesis of high-quality carbon nanodots from hydrophilic compounds: role of functional groups. Chem Commun. 2012;48(33):3984–6.
17. Sachdev A, Gopinath P. Green synthesis of multifunctional carbon dots from coriander leaves and their potential application as antioxidants, sensors and bioimaging agents. Analyst. 2015;140(12):4260–9.
18. Bhamore JR, Jha S, Park TJ, Kailasa SK. Fluorescence sensing of Cu^{2+} ion and imaging of fungal cell by ultra-small fluorescent carbon dots derived from Acacia concinna seeds. Sens Actuators B Chem. 2018;277:47–54.
19. Kumawat MK, Thakur M, Gurung RB, Srivastava R. Graphene quantum dots from Mangifera indica: application for breast cancer therapy and bioimaging. ACS Sustain Chem Eng. 2017;5(2):1382–91.
20. D'Souza SL, Deshmukh B, Bhamore JR, Rawat KA, Lenka N, Kailasa SK. Synthesis of fluorescent nitrogen-doped carbon dots from dried shrimps for cell imaging and boldine drug delivery system. RSC Adv. 2016;6(15):12169–79.
21. Su R, Wang D, Liu M, Yan J, Wang JX, Zhan Q, et al. Subgram-scale synthesis of biomass waste-derived fluorescent carbon dots in subcritical water for bioimaging and sensing. ACS Omega. 2018;3(10):13211–8.
22. Aggarwal BB, Sundaram C, Malani N, Ichikawa H. Curcumin: the Indian solid gold. Adv Exp Med Biol. 2007;595:1–75.
23. Pattnaik S, Subramanyam VR, Bapaji M, Kole CR. Antibacterial and antifungal activity of aromatic constituents of essential oils. Microbios. 1997;89(358):39–46.
24. Subapriya R, Nagini S. Medicinal properties of neem leaves: a review. Curr Med Chem Anticancer Agents. 2005;5(2):149–56.
25. Gupta SC, Patchva S, Aggarwal BB. Therapeutic roles of

Journal of Molecular Science
Volume 36 Issue 1, Year of Publication 2026, Page 252-258
DoI-10.004687/1000-9035.2026.032

curcumin: lessons learned from clinical trials. AAPS J. 2013;15(1):195–218.
26. Wang Q, Huang X, Long Y, Wang X, Zhang H, Zhu R, et al. Hollow luminescent carbon dots for drug delivery. Carbon. 2013;59:192–9.
27. Mewada A, Pandey S, Thakur M, Jadhav D, Sharon M. Swarming carbon dots for folic acid mediated delivery of doxorubicin and biological imaging. J Mater Chem B. 2014;2(6):698–705.
28. Qu K, Wang J, Ren J, Qu X. Carbon dots prepared by hydrothermal treatment of dopamine as an effective fluorescent sensing platform for the label-free detection of iron(III) ions and dopamine. Chemistry. 2013;19(22):7243–9.
29. Zhu S, Meng Q, Wang L, Zhang J, Song Y, Jin H, et al. Highly photoluminescent carbon dots for multicolor patterning, sensors, and bioimaging. Angew Chem Int Ed Engl. 2013;52(14):3953–7.
30. Wang B, Tang W, Lu H, Huang Z. Hydrothermal synthesis of carbon dots from Coriandrum sativum and their application as a fluorescent sensor for Fe^{3+} and biocompatible bioimaging. RSC Adv. 2015;5(49):39172–9.
31. Yang ST, Cao L, Luo PG, Lu F, Wang X, Wang H, et al. Carbon dots for optical imaging in vivo. J Am Chem Soc. 2009;131(32):11308–9.
32. Bao L, Zhang ZL, Tian ZQ, Zhang L, Liu C, Lin Y, et al. Electrochemical tuning of luminescent carbon nanodots: from preparation to luminescence mechanism. Adv Mater. 2011;23(48):5801–6.
33. Ren H, Yan T, Chen W, Liu R, Yang Y. Plant-based carbon dots: synthesis, properties, and biomedical applications. Materials (Basel). 2023;16(11):4181.
34. Yadav PK, Chandra S, Kumar V, Kumar D, Hasan SH. Carbon quantum dots: synthesis, structure, properties, and catalytic applications for organic synthesis. Catalysts. 2023;13(2):422.
35. Mintz KJ, Zhou Y, Leblanc RM. Recent development of carbon quantum dots regarding their optical properties, photoluminescence mechanism, and core structure. Nanoscale. 2019;11(11):4634–52.
36. Doshi M, Treglia A, Copur G, Chowdhury T, Pradhan AK. Photoluminescent carbon dots from chemical and natural sources for sensing and imaging applications. Nanomaterials. 2024;14(2):131.
37. Pillar-Little TJ, Wanninayake N, Nease L, Heidary DK, Glazer EC, Kim DY. Superior photodynamic effect of carbon quantum dots through facile synthesis. Carbon. 2018;140:616–23.
38. Singh I, Arora R, Dhiman H, Pahwa R. Carbon quantum dots: synthesis, characterization and biomedical applications. Turk J Pharm Sci. 2018;15(2):219–30.